Université de Mons
Faculté Polytechnique – Service de Mécanique Rationnelle, Dynamique et Vibrations
31, Bld Dolez - B-7000 MONS (Belgique)
065/37 42 15 – georges.kouroussis@umons.ac.be

G. Kouroussis, K. E. Vogiatzis, D. P. Connolly, A hybrid numerical-experimental assessment of railway ground vibration in urban area, *Proceedings of the First International Conference on Rail Transportation*, Edinburgh (UK), Chengdu (China), July 10-12, 2017.

First International Conference on Rail Transportation
Chengdu, China, July 10-12, 2017

A hybrid numerical-experimental assessment of railway ground vibration in urban area

Georges KOUROUSSIS[1], Konstantinos E. VOGIATZIS[2] and David P. CONNOLLY[3]

[1.] *University of Mons, Faculty of Engineering, Department of Theoretical Mechanics, Dynamics and Vibrations, Place du Parc 20, 7000 Mons, Belgium*

[2.] *University of Thessaly, Department of Civil Engineering, Laboratory of Transportation Environmental Acoustics, Pedion Areos, Volos 383 34, Greece*

[3.] *Heriot-Watt University, Institute for Infrastructure and Environment, Edinburgh EH14 4AS, United Kingdom*

Abstract: A common source of railway-induced ground vibrations is local defects such as rail joints, switches and turnouts which cause large amplitude excitations at isolated locations along the track. Moreover, the distance between railway networks (tram, metro) and neighbouring buildings is relatively close in urban areas. To analyse such situations, a combined numerical-experimental study is developed in this paper. The numerical approach addresses vehicle-track dynamics by considering the effect of local defects at the rail surface when a tram passes. A multibody vehicle model and a flexible two-dimensional track are coupled, which faithfully capture the interaction between the railway vehicle and the track. Field experiments are undertaken to determine track-ground dynamics. These involve measuring single source transfer mobilities between soil or building, and the force generated at the rail head, at the location of a local defect. The influence of building type and location is evaluated through experimental data collected in Brussels (Belgium). The results show that it is possible to assess vibrations from light rapid transit systems, while considering local rail defects as potential sources of vibration, and/or the complex paths associated with vibration transmission.

Keywords: ground vibration; impact force; measurement on building; turnout; rail joint; Brussels tram

1 Introduction

Modern tram and metro networks represent an interesting modal transfer by improving the quality of life of people by significantly alleviating traffic congestion and pollution, especially in urban area. However, residents are often exposed to railway vibrations. Considerable efforts have been made in order to reduce the generated vibrations in many areas, from designing mitigation solutions (e.g. on the vehicle (Nielsen et al., 2015), at the wheel/rail interface (Talbot, 2014), on the trackbed (Vogiatzis, 2010) or at the receptor (Talbot, 2016)), but some specific locations require intensive vibration assessment. Local defects, especially turnouts and rail joints, when designed poorly, are often the origin of high levels of vibration. As pointed out by Connolly et al. (2016), several actions are preferred at the rail track structure (active mitigation), rather than the implementation of a more passive solution in the far-field.

Predicting ground-borne vibrations in existing and new situations is challenging due to the lack of information of many configuration parameters, especially regarding the soil configuration. In such cases, the use of dynamic transfer functions to characterize the track/soil subsystem offers a rapid way to evaluate the amplification factors of soil. The technique developed by Nelson and Saurenman (1987) for predicting ground borne

noise and vibration caused by railway vehicles follows this idea. The main focus of this tool is to estimate the ground-borne noise and vibration between 6.3 - 200 Hz in residential areas near at-grade and subway tracks. The problem is reduced to estimating ground surface vibration with the help of the line transfer mobility, defined as a function of the frequency *f*,

$$M_{L,i} = 10\log_{10}\left(d\sum_{j=1}^{l} M_{i,j}\right) \quad (1)$$

where d is the distance between each source considered and $M_{i,j}$ is one of the l point source transfer mobilities between points i and j (Figure 1). The line transfer mobility is often defined using decibel scales. The force density L_F can be obtained from tests (as suggested by Federal Railroad Administration of the U.S. Department of Transportation (1998)) or using numerical data, as proposed by Verbraken et al. (2011). The resulting vibration is calculated at distance y_i from the track to predict the vibration velocity level

$$L_{V,i} = L_F + M_{L,i} \ . \quad (2)$$

Other scoping approaches are also available using a neural network approach coupled with a numerical model that predicts vibration levels in terms of velocity decibels, and is able to take the soil properties and multi-layered strata into account (Connolly, Kouroussis, Giannopoulos, Verlinden, Woodward and Forde, 2014; Connolly, Kouroussis, Woodward, Verlinden, Giannopoulos and Forde, 2014), which is a more efficient tool for high-speed network predictions.

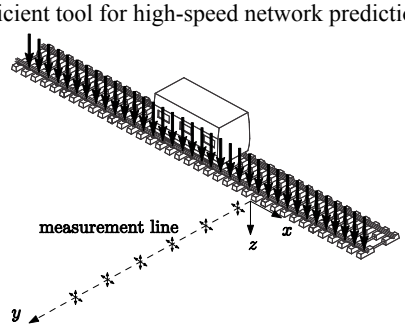

Fig. 1 Setup for vibration propagation tests for distributed sources (line transfer excitation)

However, these methods give results only when a distribution excitation is considered, neglecting local excitations (typically the high-speed lines). The situation is significantly different in the case of urban transit, due to the presence of local defects which induce elevated and localised vibrations (Kouroussis et al., 2015a, 2015b). The use of line transfer mobilities is not suitable for the present case as the periodicity assumption has not been verified. The objective of this paper is to show that source transfer mobility functions can be used to assess the vibration levels generated by local defects. A hybrid numerical/experimental prediction model is described and presented with an illustrative case from Brussels, focusing on the effect of local defects at various locations inside the Brussels region.

2 Hybrid numerical/experimental prediction model

2.1 Step 1: Predicting the wheel/rail forces using a vehicle/track/foundation model

The prediction vehicle/track/foundation model is summarized in Figure 2. Derived from the model of Zhai and Sun (1994), it consists of the classical multibody approach for the vehicle coupled with a finite element/lumped mass model for the track. The latter model lies on the foundation represented by a coupled lumped mass (CLM) model. The system is described by its mass, damping, and stiffness matrices built from its mechanical and geometrical properties. This offers a way to accurately predict the track response in low frequencies where the foundation plays an important role with non-negligible motion and a stronger coupling (Kouroussis and Verlinden, 2015).

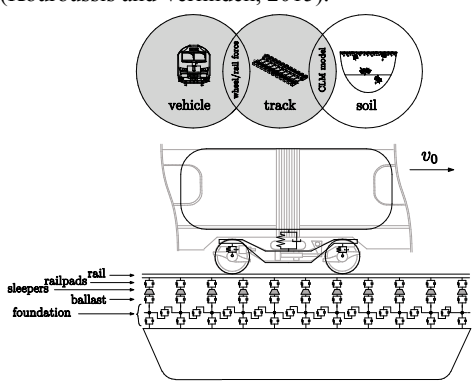

Fig. 2 Vehicle/track/foundation simulation model (Olivier et al., 2016)

The track is defined as a rail modelled by a Euler–Bernoulli beam, and discretely supported sleepers. The degrees of freedom of the vehicle are in the same plane as the track. The flexible rail is modelled with the finite element method. The sleepers have a lumped mass, and a constant spacing between each sleeper. Viscoelastic properties are considered for the railpads and ballast, which is characterised by springs and dampers. The wheel/rail contact forces are defined to couple both the vehicle and track subsystems, explicitly considered as non-linear and dependent on the wheel position and its contact to the rail

$$F_{wheel/rail,i} = K_{Hz}(z_{wheel,i} - z_{rail}(x_j) - h_{defect})^{3/2} \quad . \quad (3)$$

This connection force depends on the vertical position $z_{wheel,i}$ of the wheel and the corresponding vertical displacement $z_{rail}(x_j)$ of the rail at coordinate x_j. K_{Hz} is the Hertz's coefficient (in N/m$^{2/3}$). The vertical dynamic response of the vehicle/track subsystem due to the rail irregularity h_{defect} is therefore calculated, including the geometry of the studied local defect (represented by an analytical function) and the wheel curvature.

The simulation of the vehicle/track/foundation system is made in the time domain when the vehicle runs at a speed v_0 (assumed to be constant in the present work), with the help of a home-made C++ library called EasyDyn (Verlinden et al., 2013). As an alternative to Winkler's foundation, a CLM model has been developed for the track/soil coupling (Kouroussis et al., 2011). As the name suggests, this model takes into account the coupling between foundations, representing the contact soil area supporting the sleeper through the ballast.

The wheel/rail contact forces $F_{wheel/rail,i}$ acting on the defect location is saved during the simulation. These forces are used to define the force density L_F to characterize the excitation forces generated by the interaction of the vehicle with the local defect.

2.2 Step 2: Soil mobility transfer estimation

The basis of this method is the measurement of a single source transfer mobility function between various points *i* on a system. This function gives, as its name suggests, the transfer dynamic characteristics between two points of the system — the soil velocity response X_i and the force F_j acting at the soil surface — and yields soil dynamic information in the frequency domain (Bovey, 1983). A single source transfer mobility is theoretically defined by

$$M_{i,j} = \frac{X_i}{F_j} \quad . \quad (4)$$

Regarding the aforementioned railway-induced ground vibration problem, as the number of point transfer mobilities is increases, the better the calculation given by Eq. (1) can be used to assess the problem of distributed irregularities along the track and/or the effects of a high-speed train. However, if the study is focused on low speeds and the dynamic effect of local defects, one-point transfer mobility remains sufficient to evaluate the vibratory effects of ground wave propagation. This second case is truly applicable to urban environments (Figure 3).

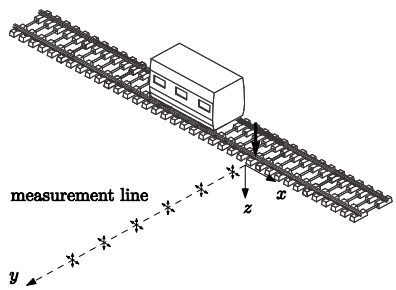

Fig. 3 Setup for vibration propagation tests for local sources of excitation.

In order to generate the transfer mobility function $M_{i,j}$ between two points *i* and *j*, simultaneous analyses must be performed on data signals representing the input force applied at one point *i* of the system (usually by performing an impulse load/impact force) and the system response motion measured at a different point *j*

$$M_{i,j} = \frac{S_{F_j X_i(f)}}{S_{F_j F_j(f)}} \quad (5)$$

where auto-spectrum of the excitation $S_{F_j F_j(f)}$ and cross-spectrum of excitation and response $S_{F_j X_i(f)}$ are defined as

$$S_{F_jF_j(f)} = \frac{1}{n}\sum_{k=1}^{n} F_j^*(f)F_j(f) \quad (6)$$

$$S_{F_jX_i(f)} = \frac{1}{n}\sum_{k=1}^{n} F_j^*(f)X_i(f) \ . \quad (7)$$

In addition, the causal and linear relationship between the output and input can be physically reflected by the coherence function, defined as

$$\gamma^2 = \frac{\left|S_{F_jX_i(f)}\right|^2}{S_{F_jF_j(f)}\, S_{X_iX_i(f)}} \quad (8)$$

where the auto-spectrum of the response is defined as

$$S_{X_iX_i(f)} = \frac{1}{n}\sum_{k=1}^{n} X_i^*(f)X_i(f) \ . \quad (9)$$

Careful consideration needs to be given to noise and leakage when using the Fourier transform, since poor coherence is indicative of a low signal-to-noise ratio, measurement errors, non-linearity or time-variant behaviour of the structure, or a combination of the aforementioned factors. Depending on the type of measurement used to detect the response motion, the soil velocity response $X_i(f)$ may be calculated as one derivative or one integration. Robust signal processing techniques are therefore required to avoid non-physical signals associated with the integration constant or the derivative gradient inherent to the original noisy signal and the sampling rate.

Several accelerometers or geophones can be placed along a profile perpendicular to the track, and used to measure the vertical soil response (Figure 4). The distance from the track is identified from the edge of the closest rail. A first accelerometer could be placed close to the track (tram site edge) and the other at distant points of interest (e.g. near sensitive buildings, foundation walls of dwellings, etc.). If the number of sensors is sufficient, the attenuation of ground vibrations with distance can be calculated, as well as the decay of the frequency content (soil filtering) and the scattering effect of the soil heterogeneity.

The impact force may be applied to the structure by various methods. One common way to excite structures is through the use of a sledge hammer or an impacter. A dynamic impulse hammer with an embedded force sensor is an efficient exciter, easy to use and very portable. It must, however, excite the structure with constant force over the frequency range of interest. Moreover, the weight of the hammer and the number of impacts impose physical requirements from the operator and a reliable series of impacts are not always necessarily obtained (Bovey, 1983). This is why a mechanical exciter in the form of a drop hammer impactor was used as an alternative. In the present work, a falling mass machine was used to perform the tests. It consists of a steel frame serving as a guidance support for a falling mass. The latter is constituted by several heavy masses (12.5 kg each) and an elastomer support to allow for the filtering to the desired frequency range. The total mass can be up to 52 kg and be launched from a maximum height of 1.5 m. A mechanical winch is used with a handle to easily raise the mass and a seat belt buckle serves as actuator. An accelerometer is placed on top of the mass to measure the mass acceleration (and the excitation force by multiplying the measured acceleration by the mass). A short analytical calculation proved that, for a nominal height of 1 m, the expected duration of the impact is 2.2 ms with a maximum acceleration of 200 g (corresponding to a maximum force of 10 tonnes), covering a frequency range up to 100 Hz.

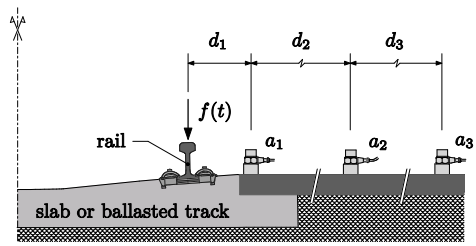

Fig. 4 Experimental setup and location of the sensors

Finally, the wheel/rail forces defined by Eq. (3) and saved during the first calculation step are combined with the mobility transfer function obtained from Eq. (5). Practically, the discrete Fourier transform is used to obtain the corresponding force spectra $F_{wheel}(f)$ (from all the forces $F_{wheel/rail,i}$ for each wheelset). The vibration level is thus obtained by multiplying these two parameters

$$V(f) = F_{wheel}(f)\, M_{i,j}(f) \quad (9)$$

or, using a decibel scale,

$$L_V = L_F + M_{S,i} \ . \quad (10)$$

An inverse discrete Fourier transform is then used to obtain the equivalent time histories.

3 Results

Experimental data from a total of 14 test locations, designated from site 1 to site 14, across the Brussels Region, were examined. All sites consisted of slab and ballasted tracks and cover most tramway networks in the Brussels region. The T2006 tram is used as a reference. This choice was motivated by the several complaints arising from this type of tram circulating in Brussels. No tram pass-by was recorded (due to the lack of availability of such a tram for all the studied sites) and only impact tests were experimentally performed.

Figures 5 and 6 presents some examples of calculated wheel/rail forces obtained from the vehicle/track/foundation model. The passing of the tram T2006 at a constant speed of v_0 = 30 km/h on a rail joint (geometrical shape of a pulse) is retained. Both positive and negative pulse joint forces are presented. The impact of each wheel is clearly visible: each axle crosses the defect at times t = 0.98 s, t = 1.19 s, t = 1.89 s, t = 2.09 s, t = 2.79 s and t = 2.99 s, with strong oscillations produced after each impact. This corresponds to a signal frequency around 16 Hz and is associated to the vehicle's bogie bounce mode.

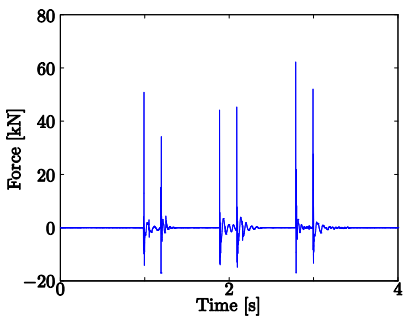

Fig. 5 Calculated wheel/rail forces acting on defect location for a tram T2006 running at 30 km/h on a rail joint (positive pulse of height 1 mm; length 5 mm)

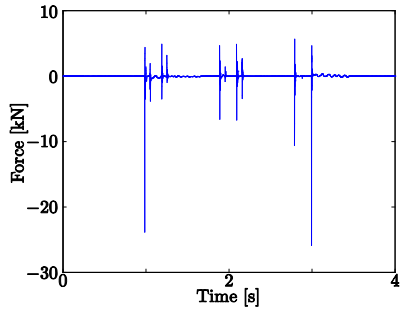

Fig. 6 Calculated wheel/rail forces acting on defect location for a tram T2006 running at 30 km/h on a rail joint (negative pulse of length 5 mm)

Figure 7 to 9 present some calculated transfer mobility functions issued from the measurement (for site 1, a ballasted track with concrete sleepers; for site 6, a ballasted track with azobe sleepers and for site 12, a concrete slab track). Coherence curves are also plotted in order to define the frequency range free from measurement errors (typically between 10 - 90 Hz). Dynamic excitation generated within the track is both filtered and dampened by the soil as it propagates. This shows an attenuation with distance for the studied frequency range: between track and building foundations, a difference of almost 10-15 dB is observable. In addition, no notable difference between ballasted tracks, including concrete or wood sleepers, were found. A mean attenuation was also approximately 15 dB. It also appears that slab tracks generally present a better vibration isolation than classic ballasted tracks. In a general way, the dynamic excitation generated within the track is both filtered and dampened by the soil as it propagates. This shows an attenuation with the distance over the entire

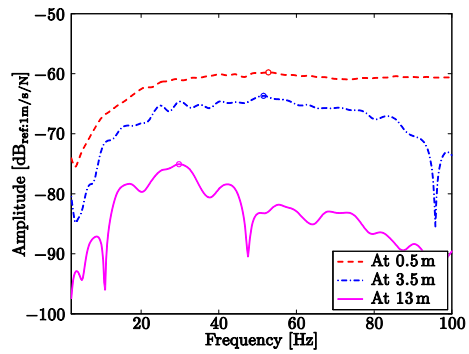

(a)

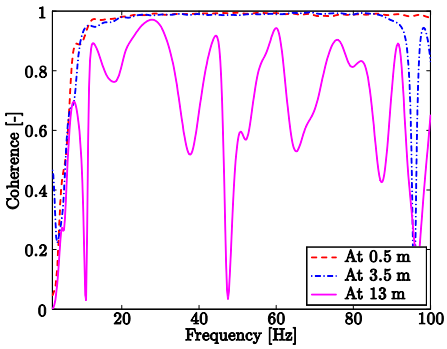

(b)

Fig. 7 Transfer mobility functions $M_{i,j}$ for site 1 (ballasted track and concrete sleepers): (a) magnitude and (b) coherence

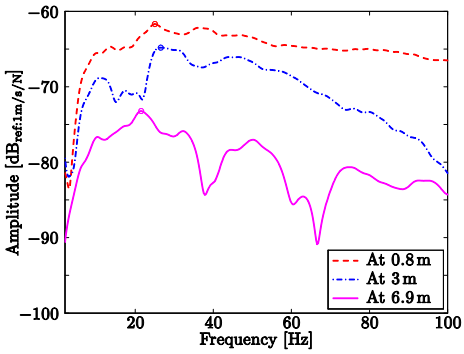

(a)

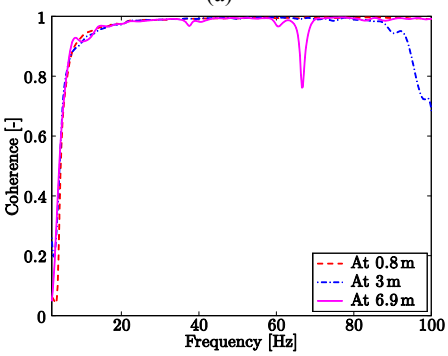

(b)

Fig. 8 Transfer mobility functions $M_{i,j}$ for site 6 (ballasted track and azobe sleepers): (a) magnitude and (b) coherence

frequency range; between track and building foundations, a difference of approximately 10-15dB is observable. Due to the limited number of measurement locations, a more affective evaluation of this attenuation was difficult to estimate. Similar trends were also found for the alternative sites.

Figure 10 shows the ground vibration results for site 1 when the tram travels over a rail joint. The response is calculated at various distances where the experimental mobility $\boldsymbol{M_{i,j}(f)}$ exists. It appears that each passing over a specific defect generates different vibration (both in shape and level). As expected, the level diminishes with distance.

Figure 11 compares the peak particle velocity (*PPV*) values calculated for each experimental site, for all the studied distances. It generally appears that slab tracks (sites 7 to 14) generally present a better vibration isolation than classic ballasted tracks (sites 1 to 6). Other findings observed from all the site results revealed that:

- A mean vibratory level at the foundation varies with the site. The maximum level does not exceed 5 mm/s, which usually represents a threshold for such buildings. Sites 9, 7 and 3 were found, in that order, to produce the highest *PPV*. Site 1 (with the higher track-foundation distance) does not present elevated vibration levels.

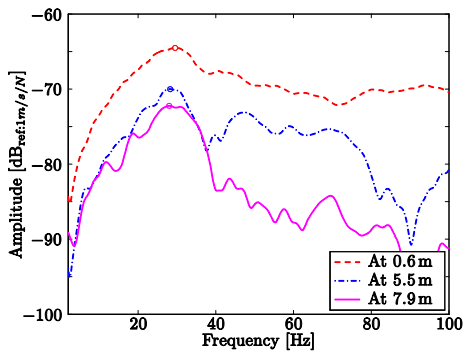

(a)

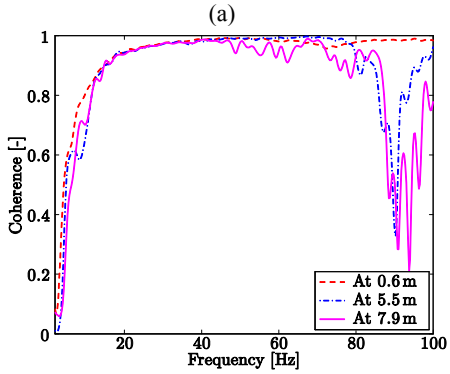

(b)

Fig. 9 Transfer mobility functions $M_{i,j}$ for site 12 (slab track and concrete sleepers): (a) magnitude and (b) coherence

- No notable difference between ballasted tracks, including concrete (sites 1 and 2) or wood sleepers (sites 3 to 6), were found.
- The only site with a floating slab, site 9, produced very high-level vibration. However, only two measurement points were used and, at this stage, it is difficult to draw significant outcomes.
- Regarding slab track sites 10 to 14 (same track-foundation distance of 7.9 m), the vibration level is relatively close between them, with the exception of site 10.

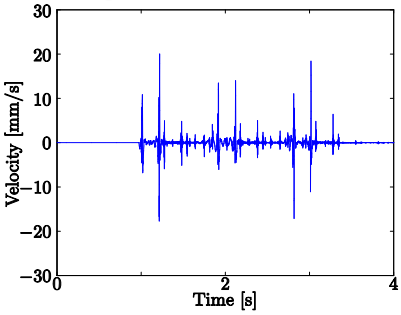

(a)

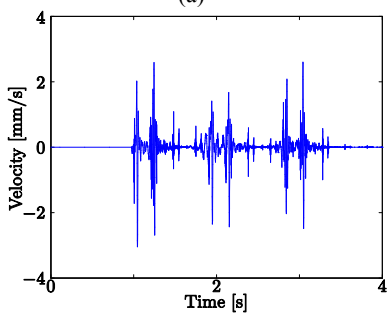

(b)

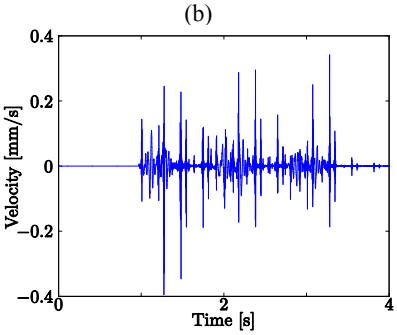

(c)

Fig. 10 Time histories of vibration velocities predicted at various distances from the track (site 1) for a tram T2006 running at 30 km/h on a rail joint (height 1 mm; length 5 mm): (a) at 0.5 m from the track, (b) at 3.5 m from the track and (c) at 13 m from the track

Figure 12 shows the peak particle velocities at the building locations as a function of defect size, considering the analysis for a step-up joint and a step-down joint. The site 7 is studied for a T2006 tram running at a constant tram speed of 50 km/h. It appears that the non-linear effects at the wheel/rail contact are evident since the two step-type defects (same wheel/rail contact definition) induce different ground vibration levels. This effect was pointed out and discussed by (Kouroussis et al., 2015b), showing with numerical results that the coupled vehicle/track dynamics have a strong influence on the vibration levels for such cases.

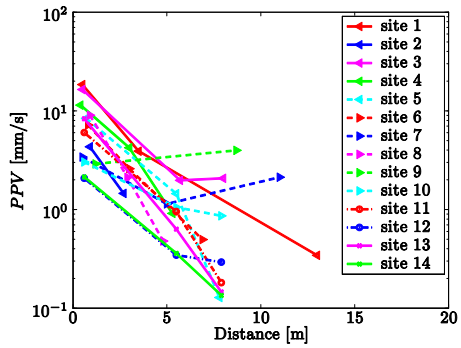

Fig. 11 Predicted *PPV* as a function of all the studied sites for a tram T2006 running at 30 km/h on a pulse joint defect (height 1 mm; length 5 mm)

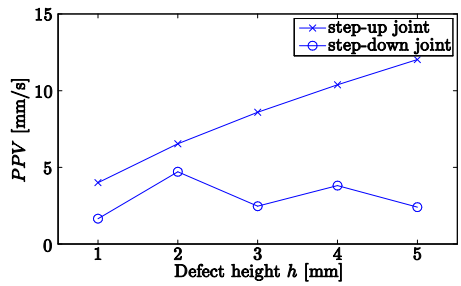

Fig. 12 Predicted *PPV* as a function of the defect size for a tram T2006 running at 50 km/h on a step-up joint or on a step-down joint (variable height)

8. Conclusions

This paper presented a hypothesis to predict railway-induced ground vibrations in the presence of singular defects. These vibrations are due to the large forces generated between wheel and rail and the location of a defect. At the early stages of a vibration assessment, it is reasonable to consider that the effect of the vehicle is localized in the area close to the defect. Further, this research shows that source mobility functions are a useful tool to assess vibration control problems relating to light rapid transit system operations.

References

Bovey, E. C. (1983). "Development of an impact method to determine the vibration transfer characteristics of railway installations." *Journal of Sound and Vibration*, 87(2): 357–370. doi: 10.1016/0022-460X(83)90575-8.

Connolly, D. P., Kouroussis, G., Giannopoulos, A., Verlinden, O., Woodward, P. K. and Forde, M. C. (2014). "Assessment of railway vibrations using an efficient scoping model." *Soil Dynamics and Earthquake Engi*neering, 58: 37–47. doi: 10.1016/j.soildyn.2013.12.003.

Connolly, D. P., Kouroussis, G., Woodward, P. K., Verlinden, O., Giannopoulos, A. and Forde, M. C. (2014). "Scoping prediction of re-radiated ground-borne noise and vibration near high speed rail lines with variable soils." *Soil Dynamics and Earthquake Engineering*, 66: 78–88. doi: 10.1016/j.soildyn.2014.06.021.

Connolly, D. P., Marecki, G., Kouroussis, G., Thalassinakis, I. and Woodward, P. K. (2016). "The growth of railway ground vibration problems — a review." *Science of the Total Environment*, 568: 1276–1282. doi: 10.1016/j.scitotenv.2015.09.101.

Federal Railroad Administration of the U.S. Department of Transportation (1998). *High-speed ground transportation. Noise and vibration impact assessment.* Technical Report 293630–1, Office of Railroad Development Washington.

Kouroussis, G., Connolly, D. P., Alexandrou, G. and Vogiatzis, K. (2015a). "The effect of railway local irregularities on ground vibration." *Transportation Research — Part D: Transport and Environment*, 39: 17–30. doi: 10.1016/j.trd.2015.06.001.

Kouroussis, G., Connolly, D. P., Alexandrou, G. and Vogiatzis, K. (2015b). "Railway ground vibrations induced by wheel and rail singular defects." *Vehicle System Dynamics*, 53(10): 1500–1519. doi: 10.1080/00423114.2015.1062116.

Kouroussis, G., Gazetas, G., Anastasopoulos, I., Conti, C. and Verlinden, O. (2011). "Discrete modelling of vertical track–soil coupling for vehicle–track dynamics." *Soil Dynamics and Earthquake Engineering*, 31(12): 1711–1723. doi: 10.1016/j.soildyn.2011.07.007.

Kouroussis, G. and Verlinden, O. (2015). "Prediction of railway ground vibrations: accuracy of a coupled lumped mass model for representing the track/soil interaction." Soil *Dynamics and Earthquake Engin*eering, 69: 220–226. doi: 10.1016/j.soildyn.2014.11.007.

Nelson, J. T. and Saurenman, H. J. (1987). "A prediction procedure for rail transportation groundborne noise and vibration." *Transportation Research Record*, 1143: 26–35.

Nielsen, J., Mirza, A., Cervello, S., Huber, P., Müller, R., Nelain, B. and Ruest, P. (2015). "Reducing train-induced ground-borne vibration by vehicle design and maintenance." *International Journal of Rail Transportation*, 3(1): 17–39. doi: 10.1080/23248378.2014.994260

Olivier, B., Connolly, D. P., Costa, P. A. and Kouroussis, G. (2016). "The effect of embankment on high speed rail ground vibrations." *International Journal of Rail Transportation*, 4(4): 229–246. doi: 10.1080/23248378.2016.1220844.

Talbot, J. P. (2014). "Lift-over crossings as a solution to tram-generated ground-borne vibration and re-radiated noise." *Journal of Rail and Rapid Transit*, 228(8): 878–886. doi: 10.1177/0954409713499015.

Talbot, J. P. (2016). "Base-isolated buildings: towards performance-based design." *Proceedings of the Institution of Civil Engineers — Structures and Buildings*, 169(8): 574–582. doi: 10.1680/jstbu.15.00057.

Verbraken, H., Lombaert, G. and Degrande, G. (2011). "Verification of an empirical prediction method for railway induced vibrations by means of numerical simulations." *Journal of Sound and Vibration*, 330(8): 1692–1703. doi: 10.1016/j.jsv.2010.10.026.

Verlinden, O., Ben Fekih, L. and Kouroussis, G. (2013). "Symbolic generation of the kinematics of multibody systems in EasyDyn

from MuPAD to Xcas/Giac." *Theoretical & Applied Mechanics Letters*, 3(1): 013012. doi: 10.1063/2.1301 3012.

Vogiatzis, K. (2010). "Noise and vibration theoretical evaluation and monitoring program for the protection of the ancient 'Kapnikarea Church' from Athens metro operation." *International Review of Civil Engineering*, 1: 328–333.

Zhai, W. and Sun, X. (1994). "A detailed model for investigating vertical interaction between railway vehicle and track." *Vehicle System Dynamics*, 23 (supplement): 603–615. doi: 10.1080/00423119308969544.